Dynamic Simulation of Ice Condition In the Vicinity of Locks and Dams

Lianwu Liu
Department of Civil and Environmental Engineering
Clarkson University, Potsdam, NY 13699-5710
Liul@clarkson.edu

Andrew M. Tuthill
U.S. Army Cold Regions Research and Engineering Laboratory
72 Lyme Road, Hanover, NH 03755
Andrew.M.Tuthill@erdc.usace.army.mil

Hung Tao Shen
Department of Civil and Environmental Engineering
Clarkson University, Potsdam, NY 13699-5710
Htshen@clarkson.edu

ABSTRACT

This paper reports an ongoing two-dimensional numerical ice-hydraulic model study on the dynamics of ice passage at locks and dams in the Ohio River for a generic navigation project. The numerical model is refined from the model DynaRICE, which is a coupled Eulerian-Lagrangian model. The hydrodynamics of the flow are simulated with a finite-element scheme and the ice dynamics are simulated with a Lagrangian discrete-parcel method. Simulations are carried out for a variety of lock and dam configurations and operation conditions. These simulations include ice accumulation and ice passage in the upper approach of the lock under different dam gate settings, as well as upper lock gate and guide wall configurations. The capability of high flow air bubblers to deflect and retain ice is also simulated by imposing horizontal water velocity distributions at the selected location.

1. Introduction

The location and configuration of locks and dams greatly affect ice and debris passage at the structure. For example, if the locks are located on the outside of a bend, ice and debris will tend to collect in the upper approach. Down-bound barge traffic will tend to push the ice and debris into the lock and time consuming ice lockages are often required to pass the ice.

The U.S. Army Corps of Engineers is planning to rehab or construct new locks at some of their major navigation projects during the next few decades. The Ohio River Mainstem Study is developing plans that may lead to the replacement of older 600 ft-long locks with 1200 ft-long locks on the upper Ohio River. In order for the downbound tows to align properly and avoid adverse outdraft effects from the dam, it is advantageous to have guidewalls and guardwalls that are at least as long as the 1200-ft lock chamber. These longer guardwalls will result in a much larger upper approach area accumulate ice and debris however. Currently at most projects, the only way to clear this ice is to lock it through the chamber which is extremely time consuming and results in delays to navigation.

This study uses a two-dimensional numerical ice-hydraulic model to investigate alternatives for passing ice more efficiently through the lock upper approach. The model was first validated by simulating ice accumulation processes in a representative existing structure, Montgomery Locks & Dam. The Montgomery Locks & Dam, as show in Figures 1 and 2, is located on the Ohio River about 32 miles downstream of Pittsburgh, PA. The model was then used to test alternatives for effective ice management at the proposed rehabs and new lock design. A plan view sketch of the locks and dam is shown in Figure 3. The dashed lines show the existing condition and the darkened area shows the proposed new configuration.

2. Ice Dynamic Model

The numerical model is a refined version of the model DynaRICE. The DynaRICE model (Liu et al. 1999, Shen et al. 2000, Liu and Shen 2000) is a two-dimensional model for river ice transport and jam evolution. The model considers the dynamics of surface ice transport coupled with the hydrodynamics of the flow. The ice dynamics are simulated by the discrete parcel method (DPM) with smoothed particle hydrodynamics. The water flow is simulated with a finite element method using the lumping technique and leapfrog time integration. The effects of seepage through the ice jam, as well as those due to ice booms, and other hydraulic structures are considered. The governing equations for ice transport are summarized here.

Considering the surface ice layer in the river as a continuum, the momentum equation can be written as

$$M \frac{D\vec{V}}{Dt} = \vec{R} + \vec{F}_a + \vec{F}_w + \vec{G} \qquad (1)$$

in which $\vec{V} = u\vec{i} + v\vec{j}$, ice velocity; $\frac{D}{Dt}$ = material derivative; $\frac{D\vec{V}}{Dt}$ = acceleration of ice; $M = \rho_i N t_i$ = ice mass per unit area, i.e. the two-dimensional ice mass density; x, y and t =

Figure 1. Photo of the Montgomery Locks & Dam (looking upstream)

Figure 2. Photo of the Montgomery Locks & Dam area (looking upstream)

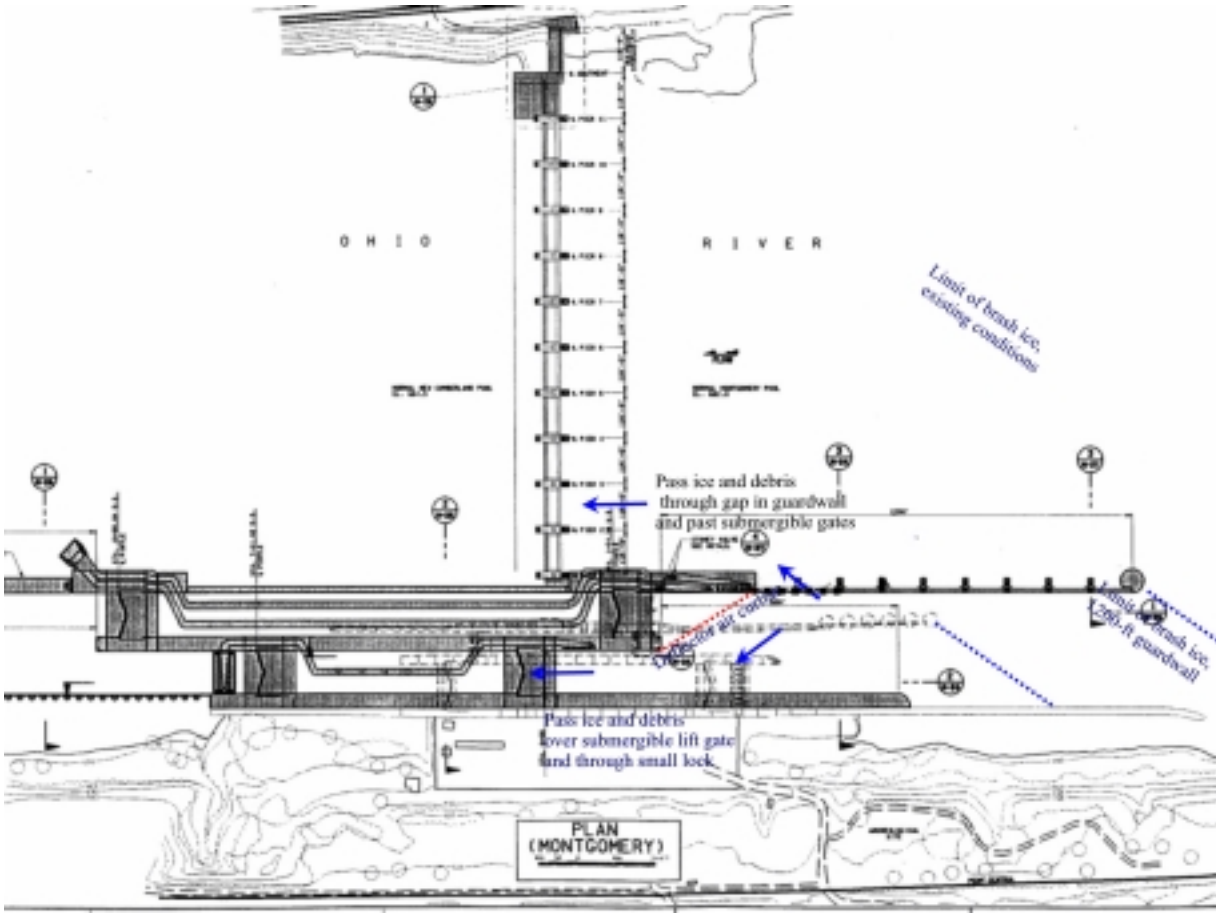

Figure 3. Plan view sketch of existing and proposed new locks at Montgomery Lock & Dam.

space and time variables; and ρ_i, N, t_i = density, area concentration, and thickness of ice, respectively; $\vec{R}$ = internal ice resistance = $\vec{i}\left[\frac{\partial}{\partial x}\left(\sigma_{xx} N t_i\right)+\frac{\partial}{\partial y}\left(\sigma_{xy} N t_i\right)\right] + \vec{j}\left[\frac{\partial}{\partial x}\left(\sigma_{yx} N t_i\right)+\frac{\partial}{\partial y}\left(\sigma_{yy} N t_i\right)\right]$, with σ_{xx}, σ_{yy} = normal stress components, and $\sigma_{xy} = \sigma_{yx}$ = shear stress components; $\vec{F}_a$ = wind drag at the air-ice interface = $N\rho_a c_a \left|\vec{W}\right|\vec{W}$, where $\vec{W} = \vec{i}W_x + \vec{j}W_y$ is surface wind velocity at 10 m above the water surface, ρ_a = density of air, and c_a = wind drag coefficient; $\vec{F}_w$ = water drag at the ice-water interface = $N\rho c_w \left|\vec{V}_w - \vec{V}\right|\left(\vec{V}_w - \vec{V}\right)$, where $\vec{V}_w$ = depth-averaged current velocity, ρ = water density, and c_w = water drag coefficient, which is a function of the ice roughness and ice and current velocities (Shen et al. 1990); and $\vec{G}$ = gravitational force due to the water surface slope $= -Mg\nabla\eta$, where η is the water surface elevation.

The ice mass conservation equation is

$$\frac{DM}{Dt} + M\nabla\cdot\vec{V} = 0 \tag{2}$$

The equation of conservation of ice area is

$$\frac{DN}{Dt} + N\nabla\cdot\vec{V} + R_a = 0 \tag{3}$$

in which, R_a = rate of change of ice area due to mechanical redistribution. Equations 2 and 3 can be combined to yield an ice thickness conservation equation:

$$\frac{\partial t_i}{\partial t} = -\vec{V} \cdot \nabla t_i + \frac{t_i}{N} R_a \tag{4}$$

A constitutive law is required to describe the ice internal stress. The widely used viscous-plastic law (Hibler 1979, Wake and Rumer 1983) was adopted in the original DynaRICE model (Shen et al. 1993).

Since rubble ice can be treated as a granular material, the yield criteria for granular material can be used for the construction of the constitutive law. In this study, the elliptical yield curve in the viscous-plastic law (Hibler 1979, Wake et al. 1983) was replaced by the commonly used Mohr-Coulomb yield criterion (Gutfraind and Savage 1997):

$$F(\sigma_1, \sigma_2) = \sigma_1 - \sigma_2 + (\sigma_1 + \sigma_2)\sin\phi = 0 \tag{5}$$

where σ_1 and σ_2 are the principal stresses and ϕ is the internal friction angle. The sign convention in continuum mechanics is used in defining positive and negative stresses; i.e. the compressive stress is defined to be negative. The internal stress can be expressed in terms of a shear viscosity μ as:

$$\sigma_{ij} = 2\mu\dot{\varepsilon}_{ij} - \mu\dot{\varepsilon}_{kk}\delta_{ij} - P\delta_{ij} \tag{6}$$

$$P = -(\sigma_1 + \sigma_2)/2 \tag{7}$$

where $\dot{\varepsilon}_{ij}$ is the strain rate tensor. Shen et al. (1990) suggested that the maximum pressure term, or the strength, could be expressed as:

$$P^* = \tan^2(\frac{\pi}{4} \pm \frac{\phi}{2})(1 - \frac{\rho_i}{\rho})\frac{\rho_i g t_i}{2}(\frac{N}{N_{\max}})^j \tag{8}$$

where, the "+" and "-" signs are for convergent and divergent states of ice flow. Assuming $\sigma_1 = -P^*$, the Mohr-Coulomb law gives

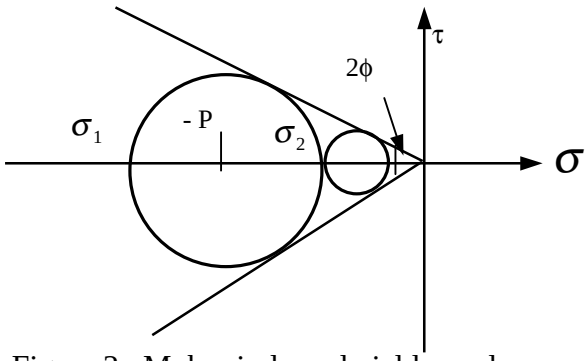

Figure 2. Mohr circle and yield envelope

$$\sigma_2 = -(1 - \frac{\rho_i}{\rho})\frac{\rho_i g t_i}{2}(\frac{N}{N_{\max}})^j \tag{9}$$

and

$$P = -(\sigma_1 + \sigma_2)/2 = \frac{1}{2}[1 + \tan^2(\frac{\pi}{4} \pm \frac{\phi}{2})](1 - \frac{\rho_i}{\rho})\frac{\rho_i g t_i}{2}(\frac{N}{N_{\max}})^j \quad (10)$$

with $\dot{\varepsilon}_1 - \dot{\varepsilon}_2 = \sqrt{(\dot{\varepsilon}_{xx} - \dot{\varepsilon}_{yy})^2 + 4\dot{\varepsilon}_{xy}\dot{\varepsilon}_{yx}}$ and Eq. 5, it can be seen that

$$\sigma_1 - \sigma_2 = 2\mu(\dot{\varepsilon}_1 - \dot{\varepsilon}_2) \quad (11)$$

Applying the Mohr-Coulomb yield criterion, Eq. 5, the shear viscosity can be expressed as

$$\mu = \frac{P\sin\phi}{\dot{\varepsilon}_1 - \dot{\varepsilon}_2} \quad (12)$$

Where $\dot{\varepsilon}_1$ and $\dot{\varepsilon}_2$ are the principal components of the strain rate tensor**.** In numerical computations, a limiting value $\mu_{\max}$ for the viscosity has to be used, since $\mu \to \infty$ when $(\dot{\varepsilon}_1 - \dot{\varepsilon}_2) \to 0$. The value of $\mu_{\max}$ can be calculated by setting a minimum value for $(\dot{\varepsilon}_1 - \dot{\varepsilon}_2)$ = $10^{-6}s^{-1}$. However, this approximation changes the constitutive relationship to a linear viscous law, and the shear stress approaches zero when the strain rate approaches zero. To avoid this problem, an elastic-plastic constitutive law is used for small strain rate conditions. In the present model, the elastic-plastic law is used when parcel velocity is smaller than 0.01 m/s.

Lu and Shen (1998) proposed a series of elastic-plastic models for small strain rates. To be consistent with the viscous-plastic law, the Mohr-Coulomb yield criterion is used here. If the bulk modulus is also neglected, the constitutive law can be written as

$$\sigma_{ij} = 2G\varepsilon_{ij} - G\varepsilon_{kk}\delta_{ij} - P\delta_{ij} \quad (13)$$

where ε_{ij} is the strain tensor, which can be obtained from time integration of the strain rate tensor. The isotropic pressure term can be expressed as in Eq. 10.

$$P = -(\sigma_1 + \sigma_2)/2 = \frac{1}{2}[1 + \tan^2(\frac{\pi}{4} \pm \frac{\phi}{2})](1 - \frac{\rho_i}{\rho})\frac{\rho_i g t_i}{2}(\frac{N}{N_{\max}})^j \quad (14)$$

Applying the Mohr-Coulomb yield criterion, Eq. 5, to describe the plastic behavior of the ice, the shear modulus can be expressed as

$$G = \frac{P\sin\phi}{\varepsilon_1 - \varepsilon_2} \quad (15)$$

Where ε_1 and ε_2 are the principal components of the strain tensor and a finite value for $G_{\max}$ is necessary for computational purpose, since $G \to \infty$ when $(\varepsilon_1 - \varepsilon_2) \to 0$. The value of $G_{\max}$ is calculated from Eq. 15 with $\varepsilon_1 - \varepsilon_2 = 10^{-6}$.

To ensure that the ice parcels at the downstream end of a naturally formed ice jam will not release due to the accuracy of numerical interpolation once the jam is initiated, a stoppage

criterion is used in the model. When an ice parcel velocity decreases to 0.1 mm/s, the parcel will be stopped. By this way the model can simulate natural ice jams formed by congestion. However, if the jam is initiated by obstacle at downstream, e.g. a stable ice cover, no stoppage criteria is needed. In this study, the stoppage condition is removed at the beginning of each hour, so that all the ice parcels will be allowed to move until they reach the stoppage criterion again.

3. Simulations of Existing Conditions

The model simulates ice accumulation and ice passage in the upper approach under a variety of dam gate settings, and upper lock gate configurations. The effect of high flow air bubblers to deflect and retain ice is also simulated by imposing horizontal water velocity distributions at locations in the model. The lock chambers and lower approach are not included in the model domain. A finite element mesh for the site includes the upper approach and the dam geometry and extends up the river about 1 mile as shown in Figure 5. Project features included in the domain are the upper gates of a 110-ft-wide landward lock and a 56-ft-wide riverward lock, a 700-ft-long solid river guardwall, and ten 100-ft-wide tainter gates. Upstream boundary conditions of the model are water and ice inflow into the river channel above the navigation project. Downstream boundaries are individual gates on the dam, the lock filling intakes, and submergible lift gates at the upper ends of the locks that act as overflow weirs to pass ice and debris. A river discharge (Q) of 45,000 cfs, is used in all simulations, representing the average mid-winter flow for the upper Ohio. Winter discharge on the Ohio River can be quite variable however. The pool is set at its normal elevation of 682.0 ft. The concentration of the initial ice parcels at the upstream boundary is 30% with a thickness of 6 in., and an area of 80 x 80 ft^2.

Case 1a. Existing geometry, even gate settings on dam

In this case the flow is uniformly distributed across all ten tainter gates, each open about 2 ft in underflow mode. Ice drifted down river, but was not allowed to pass the gates. This is based on the consideration that typically a minimum opening of about 5 ft needed to draw ice beneath this type of gate (Personal Communication with J. Anderson, Lock master, Montgomery L & D, 2/2/01). The ice accumulated and thickened in front of the dam to a maximum thickness of about 2.0 m. Ice accumulated in the upper lock approach to a thickness of about 1.0 m, as shown in Figure 6.

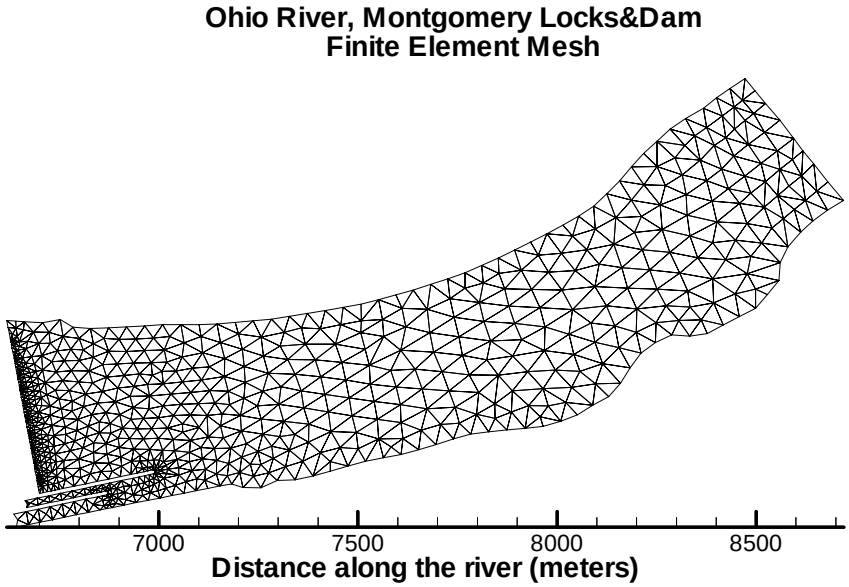

Figure 5. Finite element mesh of the model area

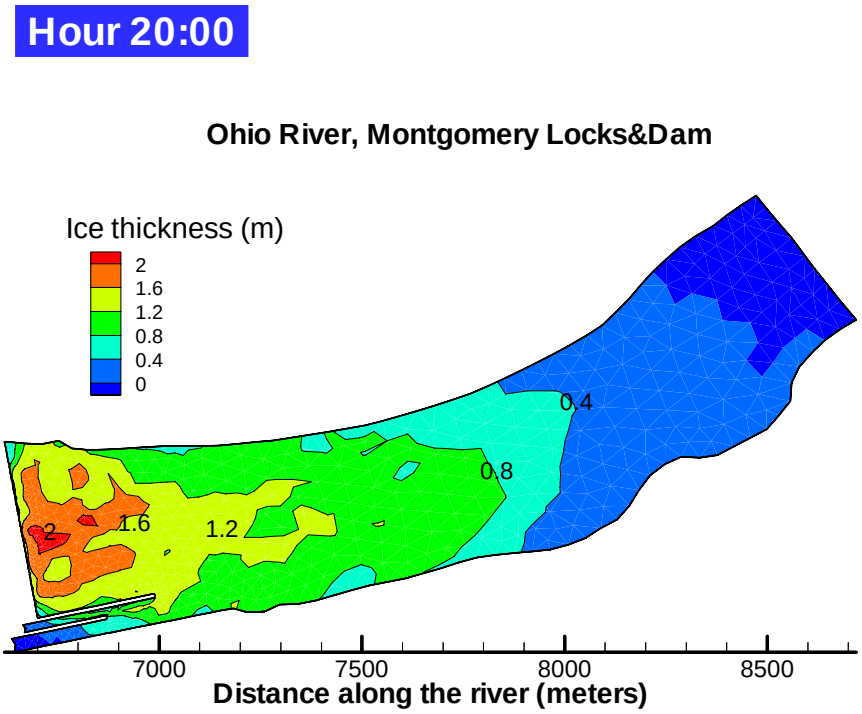

Figure 6. Simulated ice thickness of Case 1a at hour 20

Case 1b Existing geometry, water flow concentrated through gates 1 and 2

Based on the experience of lockmasters, the ice in the pool can pass the dam, if the flow is concentrated through gates 1 and 2 on the left side of the dam (directions are looking downstream). This is rarely if ever practiced, due to the potential for downstream bed scour but with improved apron design more bed protection this would be possible. . In this simulation, the flow is concentrated through gates 1 and 2, with 16,000 cfs through each gate and remainder of the 45,000 cfs distributed evenly through the other eight gates. Ice is allowed to pass gates 1 and 2 but not the other 8 gates to the right. The simulation result shows that ice passes continuously through gates 1 and 2 without arching, and the accumulation in the upper lock approach is much thinner than in Case 1a (Figures 6 and 7).

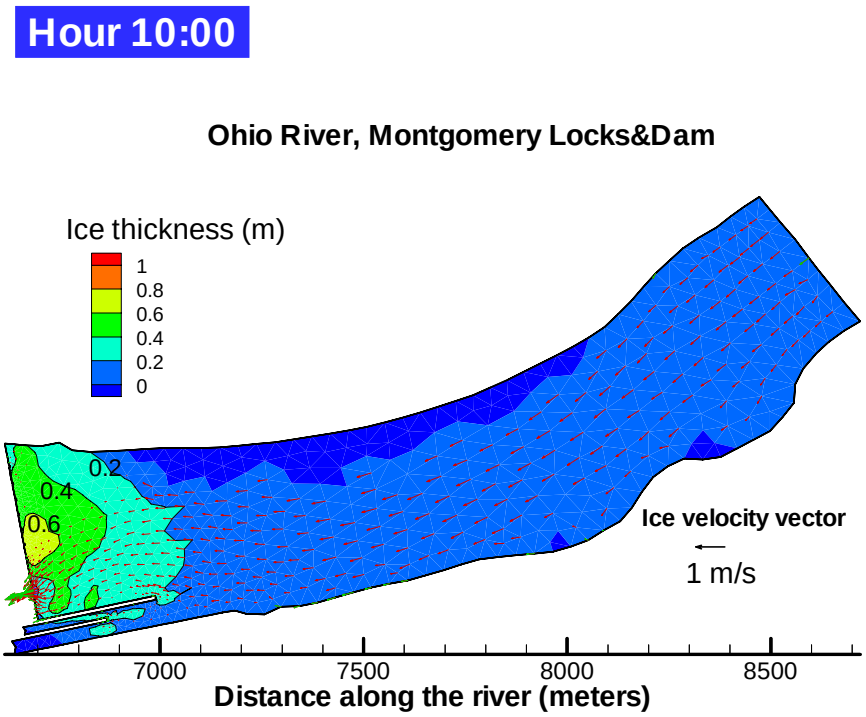

Figure 7. Simulated ice thickness and velocity of case 1b at hour 10.

4. Simulations for Proposed New Lock Configuration

The new lock configuration consists of a 1200-ft-long by 100-ft-wide riverward lock with a 1200-ft-long river guardwall, and a 600-ft-long by 110-ft-wide landward lock as shown in Figure 3. In this case, the river guardwall is modeled as a solid boundary with no underflow. Note that the left-hand spillway and gate 1 have been eliminated and a new gate 10 has been added in the location of the right-hand spillway. An important aspect of the new geometry is the 3 to 4-fold upper approach area increase for collecting ice and debris. The finite element mesh is shown in Figure 8.

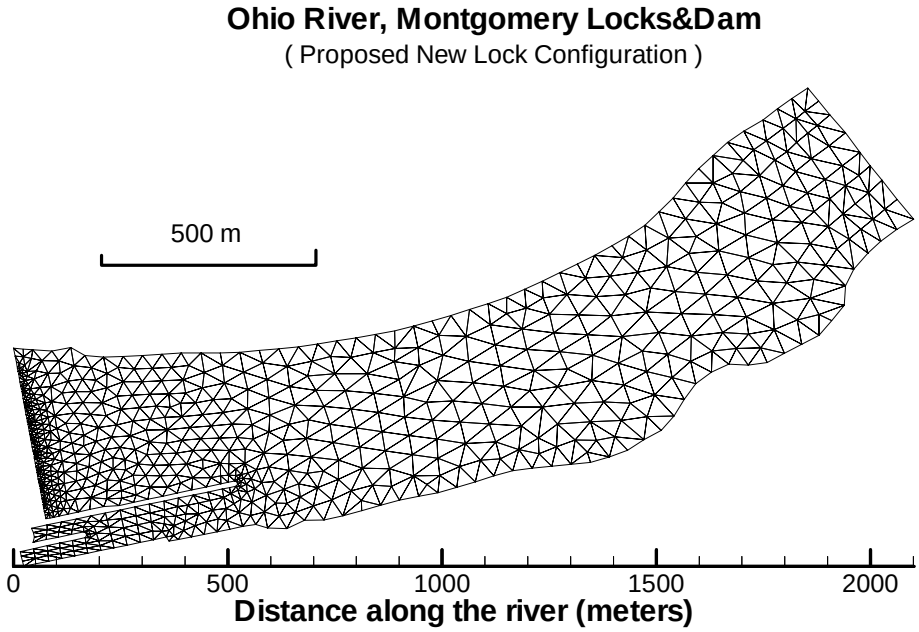

Figure 8. Finite element mesh of the model area for the proposed new configuration

Case 2a. New geometry, even gate settings on dam

This case repeats Case 1a with the new geometry to compare the ice accumulation process with the larger upper approach area to the existing condition case. The simulated ice accumulation in the upper approach is both larger and thicker than it was under existing conditions (case 1a) (Figures 7 and 9). The increase in ice thickness results from higher water velocity in the pool area outside the lock approach.

Case 2b. New geometry, water flow concentrated through gates 1 and 2

This case repeats Case 1b but with the new geometry. Due to the concentrated flow through gates 1 and 2, the ice continuously passes these gates and, similar to case 1b, does not accumulate significantly in the upper approach (Figure 10).

Case 2c. New geometry, flow concentrated through gates 1 and 2, 100 ft gap in guardwall

This case is the same as Case 2b, except that the first 100-ft span (nearest to the lock) of the upper guardwall is removed. The simulation result shows that the water current through the opening will not draw ice out of the upper approach. The high internal pressure of the ice in the pool actually pushed some ice into the upper approach, as shown in Figure 11. Another simulation (Case 2d) with the first-200ft-span of the upper gaurdwall removed gives a similar result, with ice entering rather than exiting the upper approach though the guardwall opening.

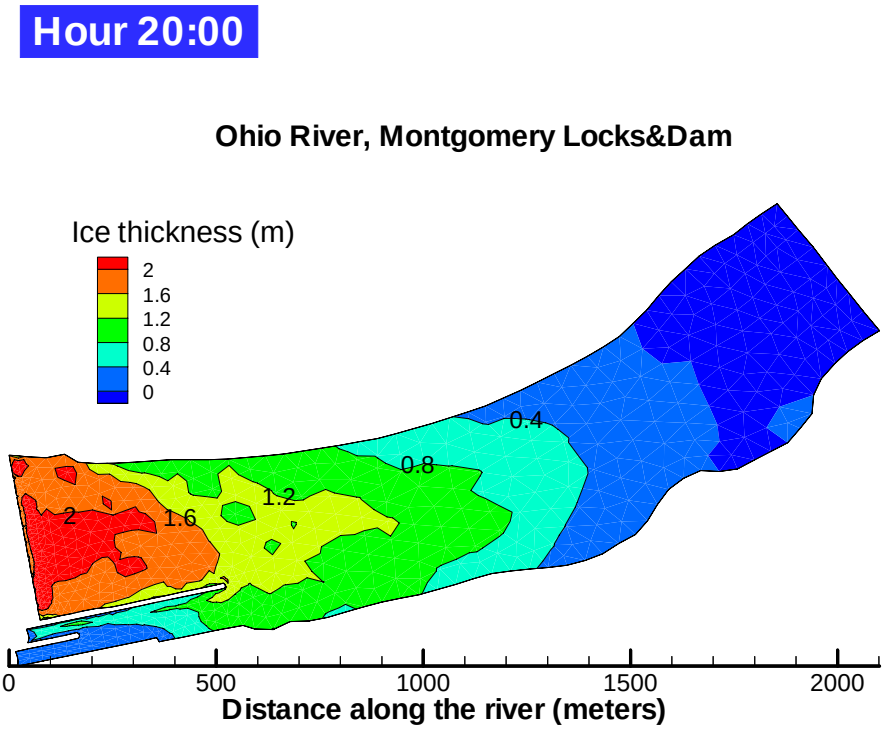

Figure 9. Simulated ice thickness of Case 2a at hour 20

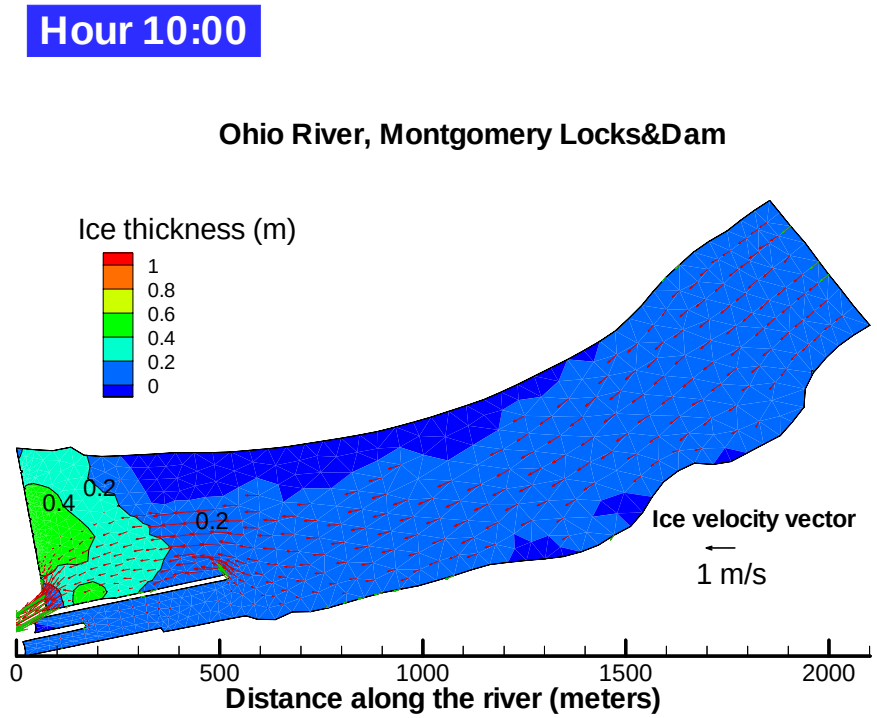

Figure 10. Simulated ice thickness and velocity of Case 2b at hour 10

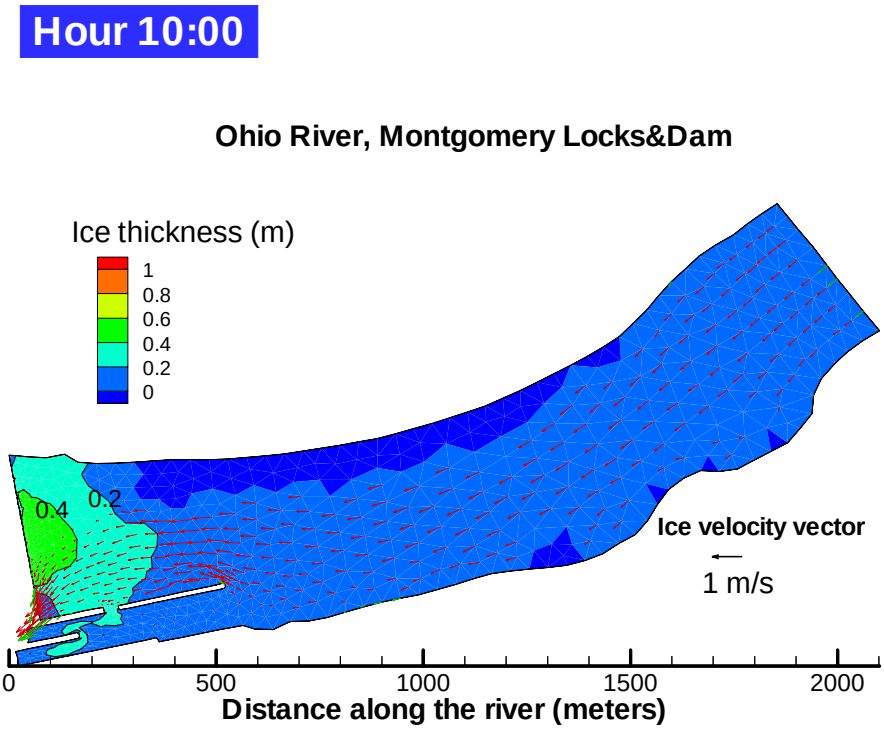

Figure 11. Simulated ice thickness and velocity of Case 2c at hour 10

Case 2e. New geometry, even gate openings on dam, ice skimming through landward lock.

Some locks are equipped with submersible lift gates or skimmer bulkheads at their upstream ends for emergency closure as well as ice and debris passage. With this equipment, it is possible to latch the miter gates open, submerge the lift gate and skim ice or debris from the upper approach through the lock chamber.

In this simulation, a water outflow boundary at the upstream end of the landward lock is specified to pass 3,000 cfs through the lock chamber and distribute the remainder of the 45,000 cfs evenly through the 10 dam gates. Starting from an ice-free river condition, the simulation shows that the arriving ice will arch at the upstream end of the upper approach causing an ice accumulation to progress upstream (Figure 12). Another simulation (Case 2f) with 6,000 cfs through the lock chamber had a similar result.

Case 2i. New geometry, even gate openings on dam, ice skimming through landward lock, diagonal air curtain to deflect ice away from entrance to riverward lock.

This simulation repeats Case 2e, but adds a diagonal air curtain across the entrance to the riverward lock to deflect ice towards the entrance of the landside lock. To simulate the effect of the air curtain, we imposed linear, 25-ft-wide velocity fields of 2 ft/s, diverging in opposite directions from the bubbler centerline. The simulation result shows that the deflector helps divert ice towards the entrance of the landward lock, and prevents ice from entering the main lock (Figure 13).

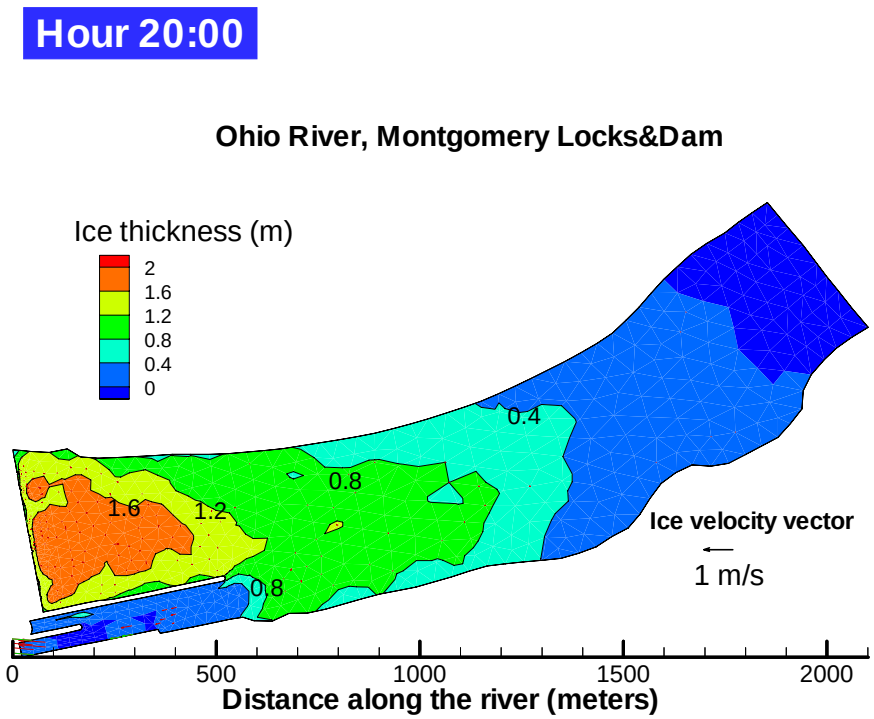

Figure 12. Simulated ice thickness and velocity of Case 2e at hour 20

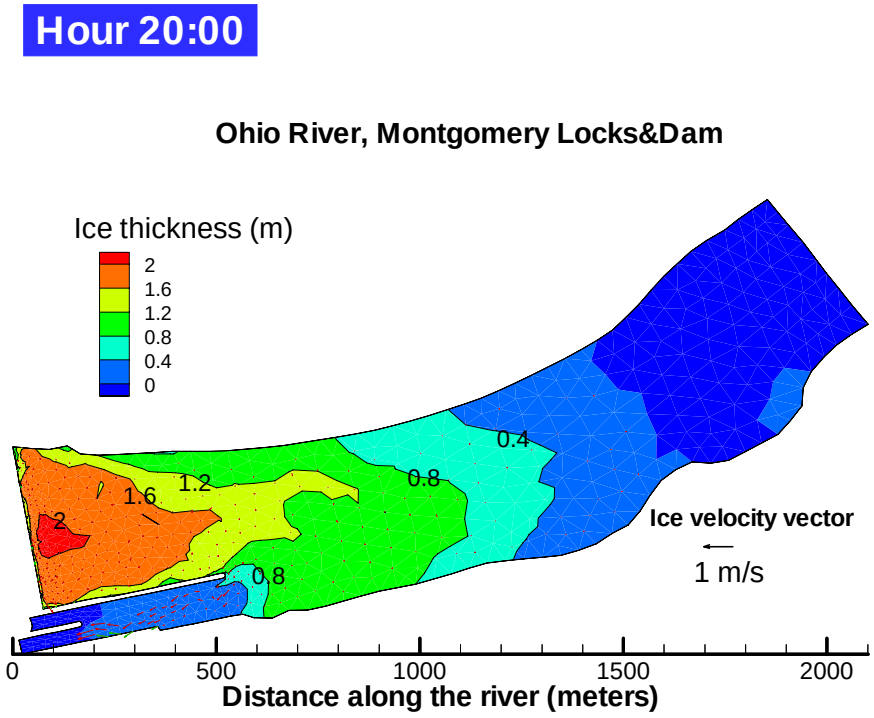

Figure 13. Simulated ice thickness and velocity of Case 2i at hour 20

5. New Lock Configuration Simulations with Pier-Supported Guardwall

The proposed river guardwall consists of pier-supported, pre-cast concrete beams. At normal pool elevation of 682 ft, the beams are submerged 2 ft and have 12 ft of freeboard. The riverbed below the guardwall is "finished" at an elevation of 646 ft, providing 34 ft water clearance below the beams. The beams are about 10 ft wide across the top and 14 ft in height. The wall is solid for the first 250 ft upstream of the riverward lock miter gates to the point where the first beam starts. There are nine beam spans supported by 10-ft-diameter concrete piers. The upstream end of the wall is a 60-ft diameter solid cell.

Since the beams are only submerged 2 ft, they can be modeled as a fixed surface barrier similar to an ice boom in the original DynaRICE model. It is assumed that when the normal velocity towards either side of the guardwall exceeds 2.25 ft/s (0.7m/s) the ice pieces will submerge and pass the guardwall. It is also quite possible that ice pieces will pass under the beams due to water drag and ice pressure, when the ice accumulation extends below the bottom of the beam, as shown in 14. In this simulation, it is assumed that the ice below the 2 ft depth will move beneath the guardwall. The ice forces on both sides of the guardwall can also be calculated.

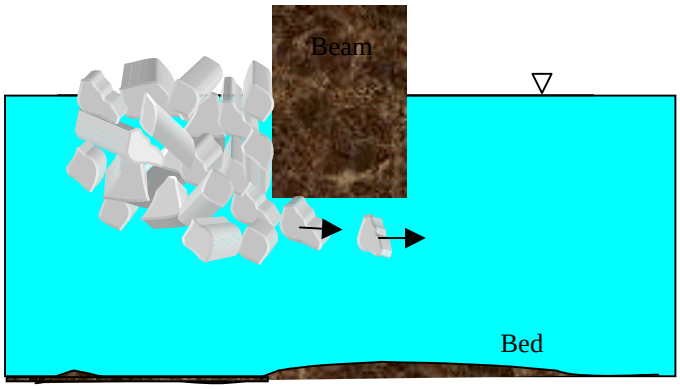

Figure 14. Sketch of ice passing under beam

Case 3a. New geometry, even gate settings on dam, flow beneath guardwall

This case repeats Case 2a with the new pier-supported guardwall design. The simulated ice accumulation, as shown in Figure 16, is similar to solid guardwall case (Figure 9) outside the upper approach, but is thicker inside the upper approach. This is because the ice can pass underneath the guardwall beam into the upper approach due to the ice pressure gradient towards the upper approach.

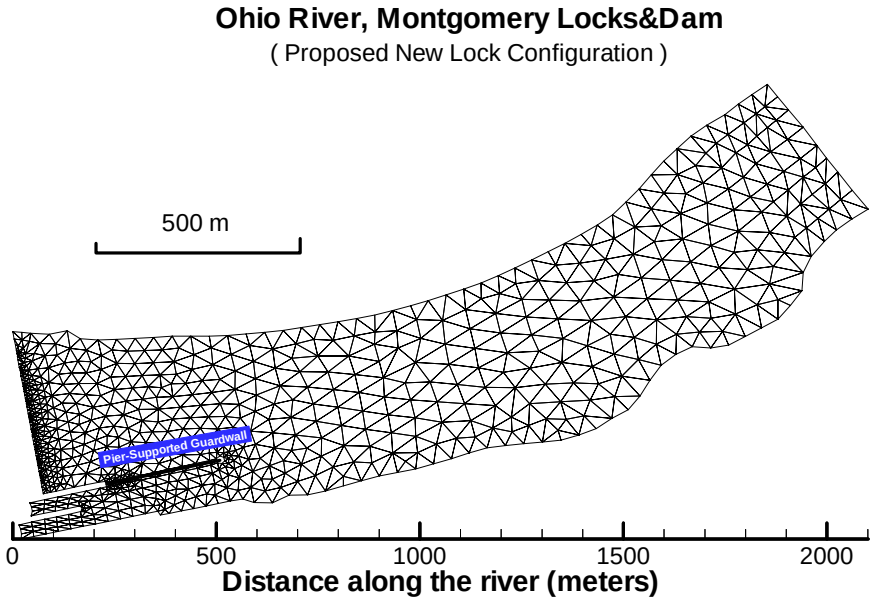

Figure 15. Finite element mesh of the model area for the proposed new configuration

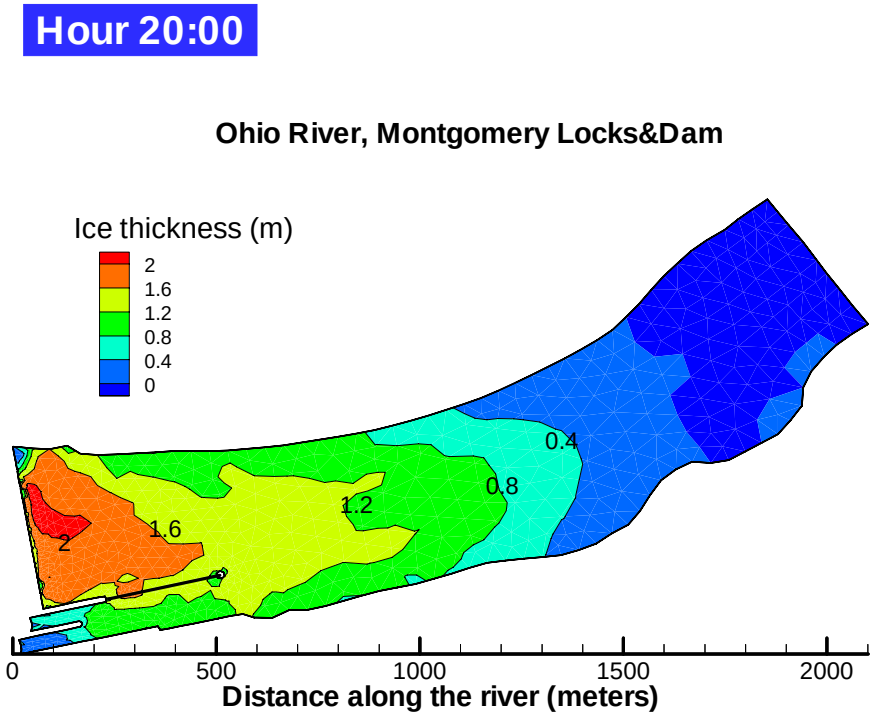

Figure 16. Simulated ice thickness of Case 3a at hour 20

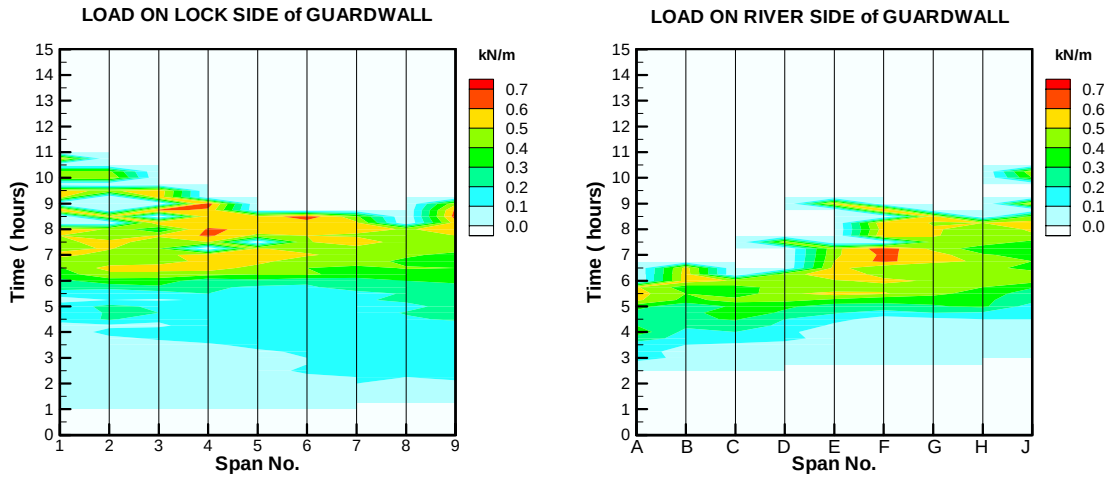

Figure 17. Contour plot for simulated forces on guardwall spans for Case 3a

The calculated time-dependent ice force distribution on both sides of the guardwall is plotted in Figure 17.

Case 3b. New geometry, flow concentrated through gates 1 &2, flow beneath guardwall

This case repeats Case 2b but with flow allowed beneath the guardwall. With flow concentrated through gates 1 and 2, more ice is drawn into the upper approach than in the even gate setting case (2a) (Figure. 18).

Case 3d. New geometry, flow concentrated through gates 1 &2, flow beneath guardwall, 200-ft gap in guardwall.

This case is the same as Case 3b, except that the first 200 ft (nearest the lock) of the upper guardwall is removed. This time, the ice supply is stopped at hour 14 to see if the current will draw ice out the upper approach through the gap. The simulation results show that ice in the upper approach can be drawn out through the 200 ft gap. In a similar simulation with a 100 gap (Case 3c), the ice arched however and was not draw out of the upper approach.

6. Summary and Conclusions

A two-dimensional ice-hydraulic numerical model is used to investigate alternatives for managing brash ice above navigation dams more efficiently and clearing ice from the upper lock approach. The model used in this study is refined from the coupled Eulerian-Langrangian model DynaRICE. Simulations were carried out for a generic navigation project on the Ohio River. The model was first validated by simulating ice accumulation processes in a representative existing structure. The model was then used to test alternatives for effective ice management for proposed rehab alternatives and new lock designs. The simulation results showed that by adding an air bubbler across the entrance to the main lock could help divert ice from entering it. The simulation results also showed that it possible is to draw ice from the upper approach by creating a gap in the upper guardwall provided there is water flow beneath. The study showed that the numerical model is an effective tool for assessing ice and debris management issues in the design of navigation locks and dams.

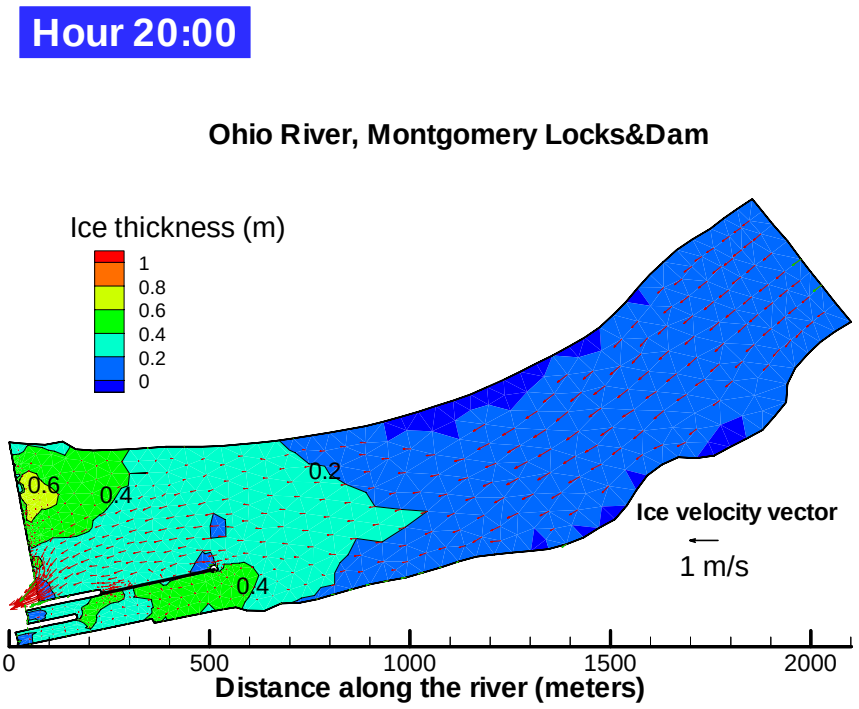

Figure 18. Simulated ice thickness and velocity of Case 3b at hour 10

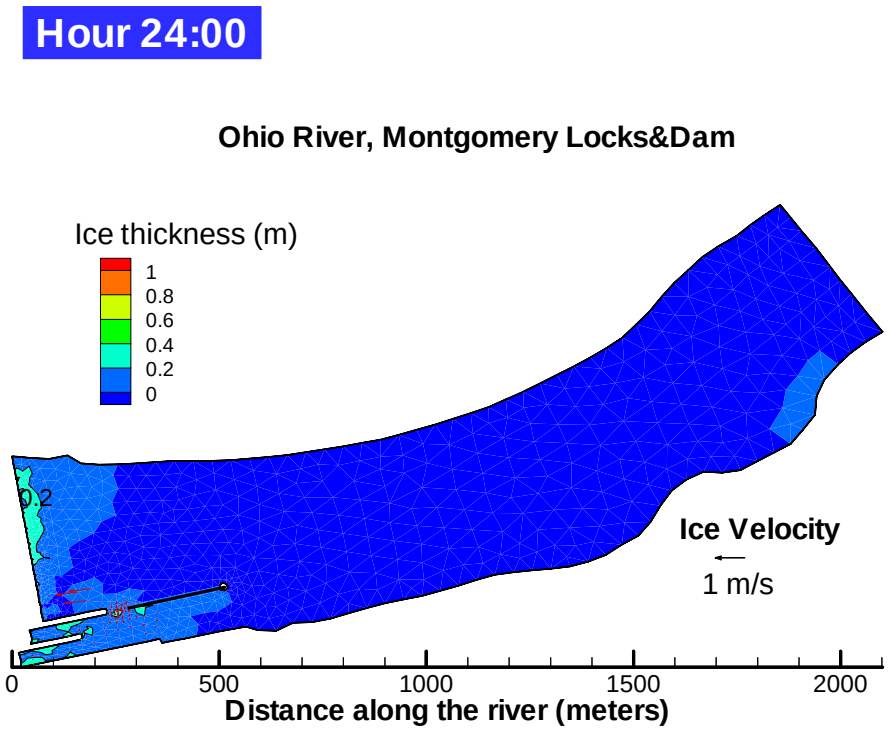

Figure 19. Simulated ice thickness and velocity of Case 3d at hour 10

Acknowledgement

This study is supported by the U.S. Army Engineering Research and Development Center, Cold Regions Research and Engineering Laboratory, through Contract No. DACW 42-00-P-0460.

References

Gutfraind, R. and Savage, S.B., 1997. Marginal ice zone rheology: Comparison of results from continuum-plastic models and discrete-particle simulations, Journal of Geophysical Research, 102(6), 12647-12661.

Hibler, W.D. III, 1979. A dynamic thermodynamic sea ice model, J. Phys. Oceanography, 9(4), 815-846.

Liu, L.W. and Shen, H.T., 2000. Numerical simulation of river ice control with booms, Report ERDC/CRREL TR-00-10, U.S. Army CRREL, Hanover, NH, 28p.

Liu, L.W., Shen, H.T., and Andrew M. Tuthill, 1999. A Numerical model for river ice jam evolution, v.2, Ice in Surface Waters, (H.T. Shen ed.), Balkema Publishers, Rotterdam, 739-746.

Lu, S.A., and Shen, H.T., 1998. Constitutive Laws for river ice dynamics, V.1, Ice in Surface Waters, (H.T. Shen ed.), Balkema Publishers, Rotterdam, 109-116.

Shen, H.T., Shen, H.H. and Tsai, S.M., 1990. Dynamic transport of river ice, Journal of Hydraulic Research, 28(6), 659-671.

Shen, H.T., Chen, Y.C., Wake, A., and Crissman, R.D., 1993. Lagrangian discrete parcel simulation of two-dimensional river ice dynamics, International Journal of Offshore and Polar Engineering, 3(4), 328-332.

Shen, H.T., Su, J., and Liu, L., 2000. “SPH Simulation of River Ice Dynamics,” Journal of Computational Physics, 165(2), 752-771.

Wake, A. and Rumer, R.R., 1983. Great Lakes ice dynamics simulation, Journal of Waterway, Port, Coastal and Ocean Engrg, ASCE, 109(1), 86-102.